Effects of Friction and Surface Tide Angle of Incidence on the Coastal Generation of Internal Tides[1]

J. G. Weigand,[2] H. G. Farmer,[3] S. J. Prinsenberg, and Maurice Rattray, Jr.

Department of Oceanography
University of Washington
Seattle, Washington

ABSTRACT

For the generation of internal waves by long surface waves, the normal-mode equations and solutions that satisfy the boundary conditions in a two-layer system are found analytically. Frictional effects decrease the amplitude of an internal wave over the shelf, changing it from a standing wave to a wave that progresses coastward and decreases the interference on the amplitude of the offshore progressive wave traveling seaward. Model studies, using a two-layer system of fresh water and saline water in a 9.9-m-long channel, gave favorable results relative to the theoretical results.

Introduction. Internal waves have been observed in practically all regions of the ocean, but their distribution and amplitudinal range have not been predictable by any simple theory. The observed dominance of internal waves of tidal period suggests that their generation mechanism might be a simple result of the surface tide encountering the coastal bathymetry. A simple theory developed from this idea can serve as a guide to an adequate observational program and can provide a basis for comparison with the results of such a program or with results of comparable model studies. Current theories of internal-wave generation of tidal period have not been adequately verified either by model experiments or by observations in the ocean.

1. Contribution No. 487 from the Department of Oceanography, University of Washington. This work was supported by the National Science Foundation under grant GP-5107.

Accepted for publication and submitted to press 10 February 1969.

2. This research was performed while the senior author was on active duty with the United States Navy as a participant in the Junior Line Officers Advanced Scientific Education Program (Burke Program). Present address: United States Navy.

3. Present address: 7427 Venice Street, Falls Church, Virginia 22043.

Davis and Patterson (1956) have reviewed the theories on the creation and propagation of internal waves that had been presented up to that time. According to their review, observed internal waves are usually of a progressive nature; however, as of that time, standing internal waves had also been observed. Later theoretical works by Rattray (1957, 1960), Ichiye (1963), and LeBlond (1966), as well as the observational work by Reid (1956) and Lambright (1964), all show evidence of coastal generation of internal waves. The theoretical papers by Rattray (1957) and LeBlond (1966) have presented investigations of the effect of friction on long internal waves, while another paper (Rattray, 1960) has presented an investigation of the generation of internal waves by tides over the continental shelf. The theory of internal-wave generation over the continental shelf by surface Kelvin waves, as developed by Ichiye (1963), is complementary to the theory herein developed rather than being a limiting case. The theoretical work by Rattray (1957, 1960) will serve as a foundation for this paper.

Experimental work so far has been done mainly by Zeilon (1913, 1934) to show qualitively the generation of internal waves. Zeilon has demonstrated that, under certain conditions, surface waves generate internal waves in passing over bottom irregularities (1913) and over a large-scale feature modeled after the continental shelf (1934). Experimental work by Weigand (1962) has given good quantitative results on internal-wave generation as predicated by the theoretical work of Rattray (1960). This ability to test simple internal-wave theories by model work has motivated expansion of Rattray's work (1960) to include the effect of (i) frictional damping of the internal-wave amplitude, (ii) surface wavelengths that are not long compared with the shelf width, and (iii) surface waves incident at oblique angles to the shelf break. The two-layer system has been used, since its simple theoretical results provide a good reference of the internal-wave generation phenomenon for continuous density structures, and the theoretical amplitudes can be easily distinguished and measured in experimental work. It is recognized, however, that a two-layer system is an idealized limiting case for a natural density distribution and that certain features present in a continuously stratified system have been omitted in the interest of simplicity. A subsequent paper will present the results for the continuously stratified case.

Theoretical Formulation. The theoretical investigation considers a two-layer system in which the density of either layer is very large compared with the density difference between the two layers. A right-handed coordinate system is used, with the x axis perpendicular outward from the beach, the y axis parallel to the beach, and the z axis positive downward from the surface. The beach and continental-shelf break are parallel so that the depth changes are independent of y. The formulation considers two separate cases, depending on whether the interface between the two layers is deeper or shallower than

the continental-shelf depth. For both cases the normal-mode equations, as obtained by combining the equations of motion and continuity, are solved with the appropriate boundary conditions. Frictional effects are not included in the formulation itself but are added later in the form of an exponential decay factor on the internal amplitude. When a time dependence of $e^{i\sigma t}$ is assumed and the notations

$$g' = \frac{\Delta\varrho}{\varrho} g \quad \text{and} \quad g'' = \left(1 - \frac{\Delta\varrho}{\varrho}\right) g$$

are used, then the equations of motion for the upper layer are:

$$i\sigma u' - fv' = -g\frac{\partial \zeta'}{\partial x}, \tag{1}$$

$$i\sigma v' + fu' = -g\frac{\partial \zeta'}{\partial y}; \tag{2}$$

the equations of motion for the lower layer are:

$$i\sigma u'' - fv'' = -g''\frac{\partial \zeta'}{\partial x} - g'\frac{\partial \zeta''}{\partial x}, \tag{3}$$

$$i\sigma v'' + fu'' = -g''\frac{\partial \zeta'}{\partial y} - g'\frac{\partial \zeta''}{\partial y}; \tag{4}$$

and the equations of continuity are:

$$\frac{\partial (h'u')}{\partial x} + h'\frac{\partial v'}{\partial y} = i\sigma(\zeta'' - \zeta'), \tag{5}$$

and

$$\frac{\partial (h''u'')}{\partial x} + h''\frac{\partial v''}{\partial y} = -i\sigma\zeta''. \tag{6}$$

A single-primed quantity refers to the upper layer and a double-primed quantity refers to the lower layer; here σ is the frequency, u and v are the horizontal components of velocity, f is twice the vertical component of the earth's angular velocity of rotation, ζ is the elevation of the upper surface of a layer, h is the layer depth, ϱ is the density, and g is the acceleration due to gravity. Elimination of u' and v' from (4)–(6) gives:

$$[h'h''g'g\nabla^2\nabla^2 + (\sigma^2 - f^2)gh\nabla^2 - (\sigma^2 - f^2)^2]\zeta' = 0, \tag{7}$$

and

$$[h'h''g'g\nabla^2\nabla^2 + (\sigma^2 - f^2)gh\nabla^2 - (\sigma^2 - f^2)^2]\zeta'' = 0, \tag{8}$$

where $h = h' + h''$ and ∇^2 is the two-dimensional Laplacian operator. Upon using the surface and internal-wave celerities c_s and c_i, respectively, of the form

$$c_s^2 = gh\left[1 - \frac{h'h''}{h^2}\frac{\Delta\varrho}{\varrho} + \cdots \left(\frac{\Delta\varrho}{\varrho}\right)^2 + \cdots\right],$$

and

$$c_i^2 = g\frac{h'h''}{h}\frac{\Delta\varrho}{\varrho}\left[1 + \frac{h'h''}{h^2}\frac{\Delta\varrho}{\varrho} + \cdots \left(\frac{\Delta\varrho}{\varrho}\right)^2 + \cdots\right],$$

(7) and (8) can be factored into the normal-mode equations by using the condition that $\nabla\varrho/\varrho \ll 1$:

$$[c_s^2\nabla^2 + (\sigma^2 - f^2)]\zeta_s' = [c_s^2\nabla^2 + (\sigma^2 - f^2)]\zeta_s'' = 0, \tag{9}$$

and

$$[c_i^2\nabla^2 + (\sigma^2 - f^2)]\zeta_i' = [c_i^2\nabla^2 + (\sigma^2 - f^2)]\zeta_i'' = 0; \tag{10}$$

here $\zeta' = \zeta_s' + \zeta_i'$ and $\zeta'' = \zeta_s'' + \zeta_i''$, using a subscript $_s$ for the surface-wave contribution and a subscript $_i$ for the internal-wave contribution to each layer's elevation. Similarly, the velocities are also separated into internal-wave and surface-wave contributions.

Solutions to the Normal-mode Equations. CASE I. INTERFACE DEEPER THAN SHELF DEPTH.

In this case (Fig. 1), the boundary conditions are:

$$(u_s')_1 = 0 \qquad \text{at} \qquad x = 0, \tag{11}$$

$$h_2'[(u_s')_2 + (u_i')_2] = d(u_s')_1 \qquad \text{at} \qquad x = l, \tag{12}$$

$$(u_s'')_2 + (u_i'')_2 = 0 \qquad \text{at} \qquad x = l, \tag{13}$$

and

$$(\zeta_s')_1 = (\zeta_s')_2 \qquad \text{at} \qquad x = l, \tag{14}$$

where a subscript $_1$ denotes the shelf area ($x \geq l$) and a subscript $_2$ denotes the ocean area ($x \geq l$); l is the shelf width and d the depth over the shelf.

The solutions of (9) and (10), subject to the boundary condition (11)–(14), yield surface standing waves:

$$(\zeta_s')_1 = 2A\cos(k_1 x - \varphi_A)e^{ij_1 y} \qquad \text{for} \quad x \leq l, \tag{15}$$

$$(\zeta_s')_2 = B_1 e^{i(k_2 x + j_2 y - \varphi_B)} + B_2 e^{i(-k_2 x + j_2 y + \varphi_B)} \qquad \text{for} \quad x \geq l, \tag{16}$$

and a progressive internal wave

$$(\zeta_i'')_2 = D_1 e^{i(-m_2 x + n_2 y + \varphi_D)}. \tag{17}$$

The phase angles φ_A, φ_B, and φ_D are:

$$\tan\varphi_A = \frac{-fj_1}{\sigma k_1},$$

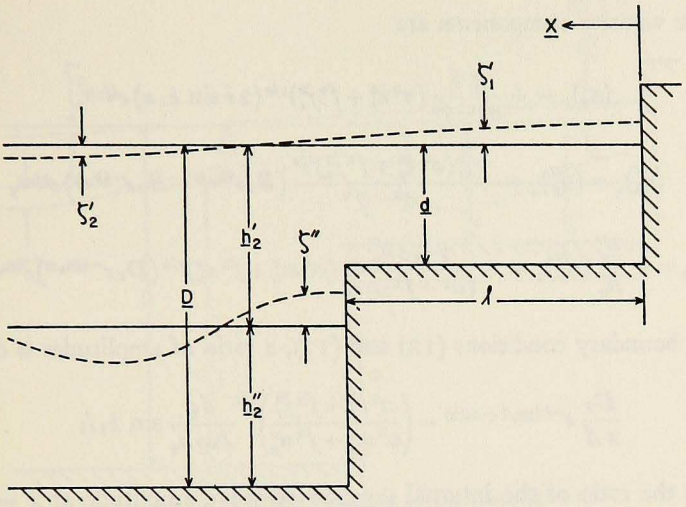

Figure 1. Model geometry used in Case I. ζ'' should read ζ_2''.

$$\tan \varphi_B = \frac{-fj_2}{\sigma k_2},$$

and

$$\tan \varphi_D = \frac{-fn_2}{\sigma m_2},$$

while the wave numbers are given by

$$k_1^2 = \frac{\sigma^2 - f^2}{gd} \cos^2 \varphi_1, \qquad j_1^2 = \frac{\sigma^2 - f^2}{gd} \sin^2 \varphi_1,$$

$$k_2^2 = \frac{\sigma^2 - f^2}{gD} \cos^2 \varphi_2, \qquad j_2^2 = \frac{\sigma^2 - f^2}{gD} \sin^2 \varphi_2,$$

$$m_2^2 = \frac{\sigma^2 - f^2}{g \Delta\varrho/\varrho} \frac{D}{h_2' h_2''} \cos^2 \psi_2, \qquad n_2^2 = \frac{\sigma^2 - f^2}{g \Delta\varrho/\varrho} \frac{D}{h_2' h_2''} \sin^2 \psi_2,$$

where the φ's and ψ's are directional angles of the waves measured from the x axis, and D is the ocean depth.

Using (1) to (6), the solutions for $(\zeta_i'')_2$ and $(\zeta_s'')_2$ are

$$(\zeta_i'')_2 = -\frac{\Delta\varrho}{\varrho} \frac{h_2''}{D} (\zeta_i'')_2, \tag{18}$$

and

$$(\zeta_s'')_2 = \frac{h_2''}{D} (\zeta_s')_2, \tag{19}$$

while the velocity components are

$$(u_s')_1 = + \frac{gA}{\sigma^2 - f^2}(\sigma^2 k_1^2 + f^2 j_1^2)^{1/2}(2i \sin k_1 x)\, e^{ij_1 y}, \tag{20}$$

$$(u_s')_2 = (u_s'')_2 = + \frac{g(\sigma^2 k_2^2 + f^2 j_2^2)^{1/2}}{\sigma^2 - f^2}(B_1 e^{ik_1 x} - B_2 e^{-ik_1 x})\, e^{ij_2 y}, \tag{21}$$

$$(u_t')_2 = -\frac{h_2''}{h_2'}(u_t'')_2 = + \frac{g \Delta\varrho h_2''}{(\sigma^2 - f^2)\varrho D}(\sigma^2 m_2^2 + f^2 n_2^2)^{1/2}(D_1 e^{-im_2 x})\, e^{in_2 y}. \tag{22}$$

By using boundary conditions (12) and (13), a ratio of amplitudes is obtained:

$$\frac{D_1}{2A} e^{-i(m_2 l + \pi/2)} = \left(\frac{\sigma^2 k_1^2 + f^2 j_1^2}{\sigma^2 m_2^2 + f^2 n_2^2}\right)^{1/2} \frac{d\varrho}{\Delta\varrho h_2'} \sin k_1 l; \tag{23}$$

this gives the ratio of the internal progressive-wave amplitude at $x = l$ to the surface standing-wave amplitude at $x = 0$.

A simple case in which the surface wave is perpendicular to the beach ($n_2 = j_1 = j_2 = 0$) reduces (23) to:

$$\frac{D_1}{2A} e^{-i(m_2 l + \pi/2)} = \left(\frac{h_2'' d\varrho}{h_2' D \Delta\varrho}\right)^{1/2} \sin k_1 l, \tag{24}$$

which can be changed to

$$\frac{D_1 e^{-i(m_2 l + \pi/2)}}{B_1 e^{ik_1 l} + B_2 e^{-ik_1 l}} = \left(\frac{h_2'' d\varrho}{h_2' D \Delta\varrho}\right)^{1/2} \tan k_1 l \tag{25}$$

$$\simeq l\left[\frac{(\sigma^2 - f^2)\varrho h_2''}{\Delta\varrho h_2' D}\right]^{1/2} \text{for small } k_1 l, \tag{26}$$

where (25) and (26) give the ratio of the internal-wave amplitude to the surface-wave amplitude at $x = l$.

Case II. Interface shallower than shelf depth.

The boundary conditions for the normal-mode equations (9) and (10) for this case (Fig. 2) are:

$$h_1'(u')_1 = h_1''(u'')_1 = 0 \quad \text{at} \quad x = 0, \tag{27}$$

$$h_1'(u')_1 = h_2'(u')_2 \quad \text{at} \quad x = l, \tag{28}$$

$$h_1''(u'')_1 = h_2'(u'')_2 \quad \text{at} \quad x = l, \tag{29}$$

$$(\zeta'')_1 = (\zeta'')_2 \quad \text{at} \quad x = l, \tag{30}$$

and

$$(\zeta')_1 = (\zeta')_2 \quad \text{at} \quad x = l. \tag{31}$$

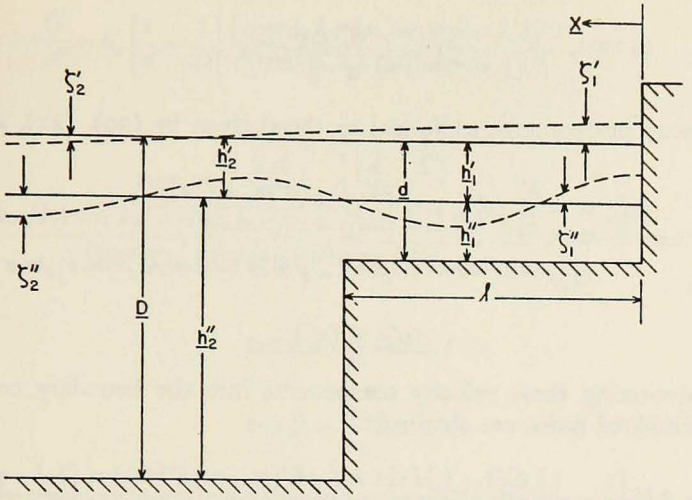

Figure 2. Model geometry used in Case II.

The solutions to the normal-mode equations and boundary conditions are wave forms as given by (15)–(19), plus an internal standing wave over the shelf $(\zeta_i'')_1$ given by

$$(\zeta_i'')_1 = C[e^{i(m_1 x + n_1 y - \varphi_C)} + e^{i(-m_1 x + n_1 y + \varphi_C)}], \tag{32}$$

where $\tan \varphi_C = (-n_1 f)/(m_1 \sigma)$ and the additional wave numbers are:

$$m_1^2 = \frac{(\sigma^2 - f^2)\varrho d}{g \Delta\varrho h_1' h_1''} \cos^2 \psi_1 \qquad n_1^2 = \frac{(\sigma^2 - f^2)\varrho d}{g \Delta\varrho h_1' h_1''} \sin^2 \psi.$$

The frictional effect is introduced here as a damping coefficient of the internal wave rather than as a Reynold's stress term in the equation of motion. The problem of damping coefficients was considered by Rattray (1957) for a two-layer fluid and by LeBlond (1966) for a continuously stratified fluid. Their results showed that the internal wave over the shelf, including the effect of friction, can be written in the form

$$(\zeta_i'')_1 = C[e^{-\mu[(l-x)/\cos\psi_1]} e^{i(m_1 x - \varphi_C)} + e^{-\mu[(l+x)/\cos\psi_1]} e^{-i(m_1 x - \varphi_C)}] e^{i m_1 y}, \tag{33}$$

where μ is the damping coefficient and $(\cos \psi_1)^{-1}$ accounts for the additional distance traveled by a wave crest making an angle ψ_1 with the shelf break.

By using (1) to (6), the other elevation components are:

$$(\zeta_s'')_1 = \frac{h_1''}{d} (\zeta_s'), \tag{34}$$

and

$$(\zeta_i')_1 = -\frac{h_1''}{d}\frac{\Delta\varrho}{\varrho}(\zeta_i'')_1. \tag{35}$$

The velocity components, additional to those given by (20), (21), and (22), are

$$\left.\begin{aligned}(u_i')_1 = -\frac{h_1''}{h_i'}(u_i'')_1 = -\frac{gh_1''\,\Delta\varrho}{d\varrho}\frac{(\sigma^2 m_1^2 + f^2 n_1^2)^{1/2}}{\sigma^2 - f^2}\\ C\left[e^{-\mu[(l-x)/\cos\psi_1]}e^{im_1 x} - e^{-\mu[(l+x)/\cos\psi_1]}e^{-im_1 x}\right]e^{in_1 y}\end{aligned}\right\} \tag{36}$$

and

$$(u_s')_1 = (u_s'')_1. \tag{37}$$

Upon substituting these velocity components into the boundary conditions, two amplitudinal ratios are obtained:

$$\frac{C}{A} = 2h_1'\left[\frac{1}{d} - \frac{1}{D}\right]\frac{G(k_1, j_1)i\sin k_1 l + G(m_2, n_2)e^{-i\varphi_D}\cos(k_1 l - \varphi_A)}{G(m_2, n_2)e^{-i\varphi_D}T(\mu) + G(m_1, n_1)S(\mu)} \tag{38}$$

and

$$\frac{D_1}{2A} = h_1'\left[\frac{1}{d} - \frac{1}{D}\right]e^{i(m_1 l - \varphi_D)}\cdot$$

$$\cdot\left[\frac{G(k_1, j_1)i\sin k_1 l + G(m_2, n_2)e^{i\varphi_D}\cos(k_1 l - \varphi_A)}{G(m_2, n_2)e^{-i\varphi_D} + G(m_1, n_1)S(\mu)T(\mu)^{-1}} - \cos(k_1 l - \varphi_A)\right], \tag{39}$$

where

$$G(a, b) = \frac{(\sigma^2 a^2 + f^2 b^2)^{1/2}}{a^2 + b^2},$$

$$T(\mu) = e^{i(m_1 l - \varphi_C)} + e^{-2\mu l/\cos\psi_1}e^{-i(m_1 l - \varphi_C)},$$

and

$$S(\mu) = e^{im_1 l} - e^{-2\mu l/\cos\psi_1}e^{-im_1 l}.$$

After multiplying (38) by $e^{-(\mu l)/(\cos\psi_1)}$, the product represents the standing-wave amplitudinal ratio of the coastal internal wave to the coastal surface wave, both observed at $x = 0$. Equation (39) represents the wave-amplitude ratio of the progressive offshore internal wave observed at $x = l$ to the coastal standing surface wave as observed at $x = 0$.

The $S(\mu)$ and $T(\mu)$ contain the frictional effect of the amplitudinal ratios and reduce to:

$$S(0) = 2i\sin m_1 l$$

and

$$T(0) = 2\cos(m_1 l - \varphi_C) \qquad \text{for } \mu = 0.$$

Thus, for a surface wave approaching the beach perpendicularly, neglecting friction, (38) and (39) respectively reduce to:

$$\frac{C}{A} = h_1' \left[\frac{1}{d} - \frac{1}{D}\right] \frac{[\cos^2 k_1 l + (m_2/m_1)^2 \sin^2 k_1 l]^{1/2}}{[\cos^2 m_1 l + (m_2/m_1)^2 m_1 l]^{1/2}} e^{i(\alpha+\beta)} \tag{40}$$

and

$$\frac{D_1}{2A} = h_1' \left[\frac{1}{d} - \frac{1}{D}\right] \cdot$$

$$\cdot \frac{[(m_2/k_1) \sin k_1 l \cos m_1 l - (m_2/m_1) \sin m_1 l \cos k_1 l]}{[\cos^2 m_1 l + (m_2/m_1)^2 \sin^2 m_1 l]^{1/2}} e^{i(\pi/2 - \beta + m_1 l)}, \tag{41}$$

where

$$\tan \alpha = \frac{m_2}{k_1} \tan k_1 l$$

$$\tan \beta = \frac{m_2}{m_1} \tan m_1 l.$$

These equations reduce further to those found by Rattray (1960) when the approximations for long surface waves, as compared with the shelf width, are used.

Experimental Procedure. Experiments were conducted in a U-shaped channel that was constructed by placing a 1.3-m-wide by 3.5-m-long rectangular box into a 2.1-m-wide by 3.9-m-long rectangular tank, as shown in Fig. 3. The U-shaped channel so constructed was 9.9 m long, 0.4 m wide, and had a 0.5-m maximum usable depth. Reflectors were placed at the two corners of the channel to reduce multiple internal-wave reflections and to assist surface-wave propagation around the corners. At one end of the channel, a vertical oscillating plunger generated low-amplitude surface waves whose period and amplitude could be controlled. The continental terrace at the other end of the channel consisted of a vertical continental slope of a fixed 29.5-cm height and of a horizontal continental shelf of 2.0-m total length. The vertical beach could be moved across the shelf to change the shelf width, l, between runs. The two-layer system consisted of a layer of fresh water over a layer of salt water, with very similar viscosity for the two layers and a density difference that could be adjusted easily.

The two-layer system was obtained by siphoning fresh water at a controlled rate onto the centers of several uniformly spaced plastic disks, the upper surface of which floated by means of cork floats level with the water surface. Two-layer density profiles, with 80% of the density change taking place in 0.5 cm, were usually obtained, and they changed to an 80% density change over a 1.0-cm depth following an afternoon of experimentation. The interface was marked by droplets of a dyed mixture of xylene and carbon tetrachloride whose density could be controlled by its fractional composition. The motions of the droplets and of the water surface could be observed through the transparent

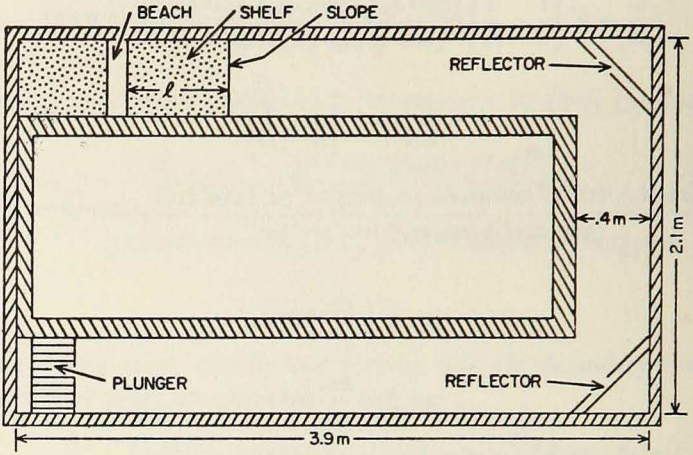

Figure 3. Plan view of the wave tank, showing the U-shaped channel and the location of the various features.

Plexiglas side of the wave tank, and the motions' amplitudes were measured at fixed values of x by means of a 0.2-cm lined transparent grid mounted over the side of the wave tank. Parallax was held to a minimum by observing the motions' amplitudes as close as possible to the observer's side of the wave tank. Figs. 4 and 5 are photographs showing representative examples of the waves observed during the experiments for Case I and Case II, respectively; the fine 0.2-cm lined grid was removed for photographic purposes.

Of greatest interest in the internal-wave generation is the dependence of the ratio of internal-wave amplitude to surface-wave amplitude, expressed as a function of the parameters of the problem. For convenience, the experimental and theoretical results are presented in terms of the shelf width. The observation of the amplitudes was made at fixed values of x; in the first case, with the interface deeper than the shelf, the amplitudes of the interface and surface movements were both measured at the shelf break ($x = l$). But in the second case, with the interface shallower than the shelf, the amplitudes of the interface movement were measured at the shelf break and at the beach; that of the surface movement was measured only at the beach. This was done so that the experimental results could be related to the theoretical results, as given by (25), (38), and (39). For each experimental setup—i.e., water depths and surface-wave frequency—runs were made with a different shelf width, l. Between each shelf-width run the beach position was changed and the water was allowed to come to a complete rest. Each run had a limited observation period, usually between 10 and 20 surface-wave periods, during which the interface movement was in a steady state. This period was between the time when a steady state was set up, usually four to six surface-wave periods, and the time when the steady state was destroyed by the appearance of the offshore

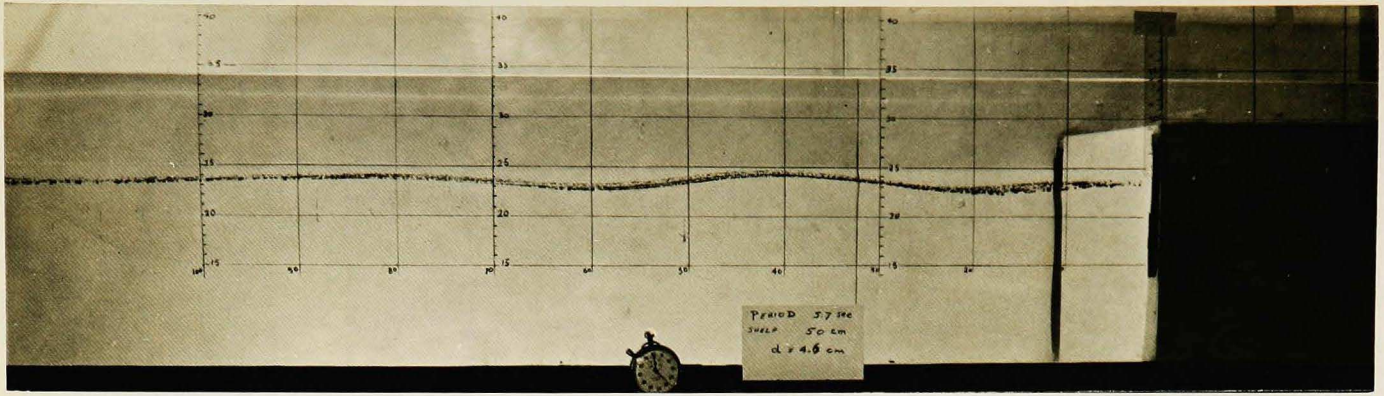

Figure 4. Typical Case I wave profile showing a progressive internal wave off the shelf; period = 5.7 sec, l = 50 cm, $\Delta\zeta/\zeta$ = 0.030, and d = 4.6 cm.

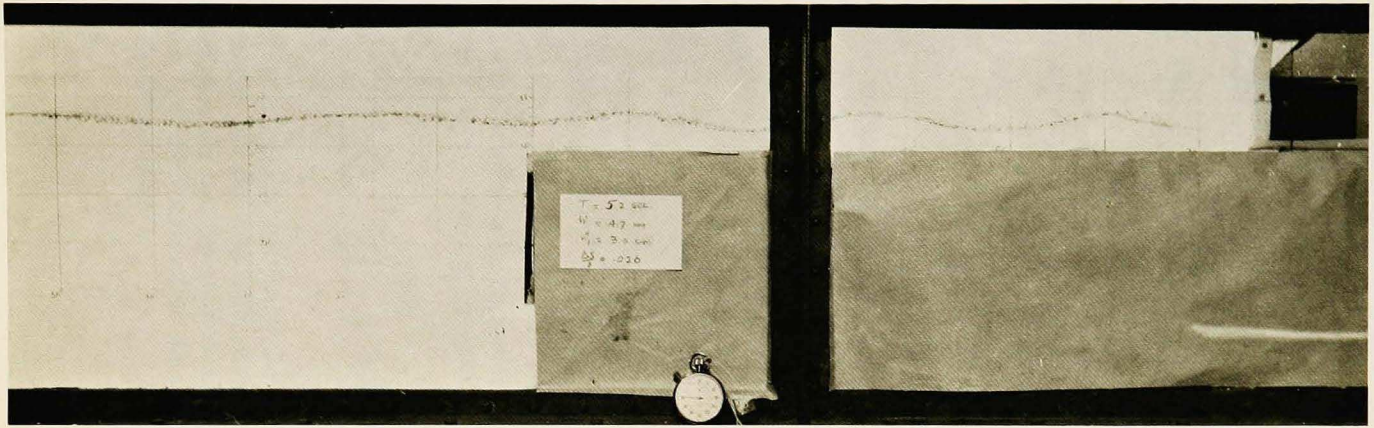

Figure 5. Typical Case II wave profile showing a progressive internal wave off the shelf and a standing internal wave on the shelf; period = 5.2 sec, l = 75 cm, $\Delta\zeta/\zeta$ = 0.026, h' = 4.7 cm, and h'' = 3.0 cm.

progressive internal wave after being reflected from the plunger. The observed surface (Z_s) and interface (Z_i) movements at fixed values of x are dependent on time only, and each consists of a summation of surface (ζ_s) and (ζ_i) modes in such a way that:

$$(Z_i)_k = (\zeta_s'')_k|_x + (\zeta_i'')_k|_x, \tag{42}$$

and

$$(Z_s)_k = (\zeta_s')_k|_x + (\zeta_i')_k|_x, \tag{43}$$

where $k = 1, 2$ refers to the shelf area (1) and the ocean area (2).

Another observed parameter is the phase angle, θ_k, between the surface and interface movements such that, at the fixed value of x,

$$(Z_i)_k = |Z_i|_k e^{i(\sigma t + \theta_k)}, \tag{44}$$

and

$$(Z_s)_k = |Z_s|_k e^{i\sigma t}. \tag{45}$$

When the effect of the internal wave on the surface movement is neglected ($\zeta_i' = 0$) and when the surface-wave effect on the interface is expressed in terms of the surface movement, we obtain the relationship:

$$(\zeta_s')_k|_x = (Z_s)_k, \tag{46}$$

$$(\zeta_s'')_k|_x = \frac{h''}{h}(\zeta_s')_k|_x, \tag{47}$$

and

$$(\zeta_i'')_k|_x = \left(|Z_i|_k e^{i\theta_k} - \frac{h''}{h}|Z_s|_k\right) e^{i\sigma t}. \tag{48}$$

Thus the theoretical ratio of the internal-wave amplitude to surface-wave amplitude at a position x is related to measurable parameters at the position x by:

$$\left.\frac{(\zeta_i'')_k}{(\zeta_s')_k}\right|_x = \frac{\left[(|Z_i|_k)^2 - 2|Z_i|_k(\cos\theta_k)\frac{h''}{h}|Z_s|_k + \left(\frac{h''}{h}|Z_s|_k\right)^2\right]^{1/2}}{|Z_s|_k}. \tag{49}$$

The effect of friction was introduced only as a damping coefficient for the internal wave over the shelf area. To determine the effective eddy viscosity and thus the damping coefficient in the model, separate experiments are needed to measure large internal-wave damping over wide shelf areas. The damping coefficient, μ, can then be calculated from the relationship

$$\mu l = \cosh^{-1}\frac{|\zeta_i''|_{x=l}}{|\zeta_i''|_{x=0}}. \tag{50}$$

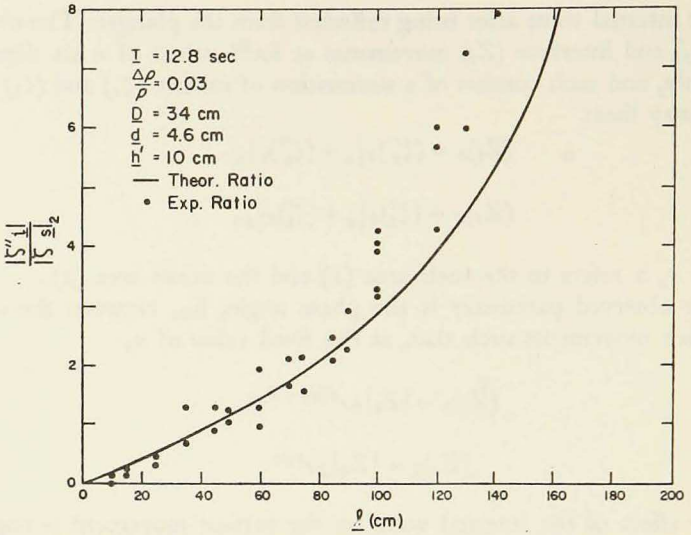

Figure 6. Theoretical and experimental ratio of internal-wave to surface-wave amplitudes of Case I for a 215-cm surface wavelength.

Experimental Results. In Figs. 6–11, ratios of internal-wave amplitudes to surface-wave amplitudes are plotted as the ordinate; the shelf width, l, is plotted as the abscissa. Figs. 6 and 7 show the theoretical results as given by

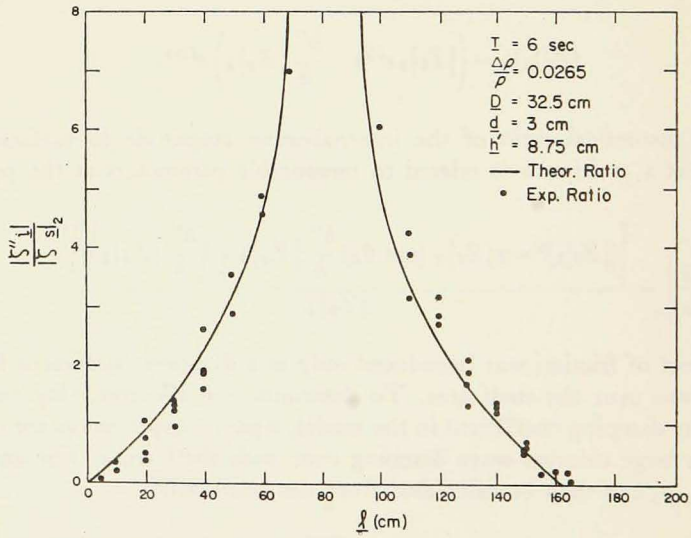

Figure 7. Theoretical and experimental ratio of internal-wave to surface-wave amplitudes of Case I for an 81-cm surface wavelength.

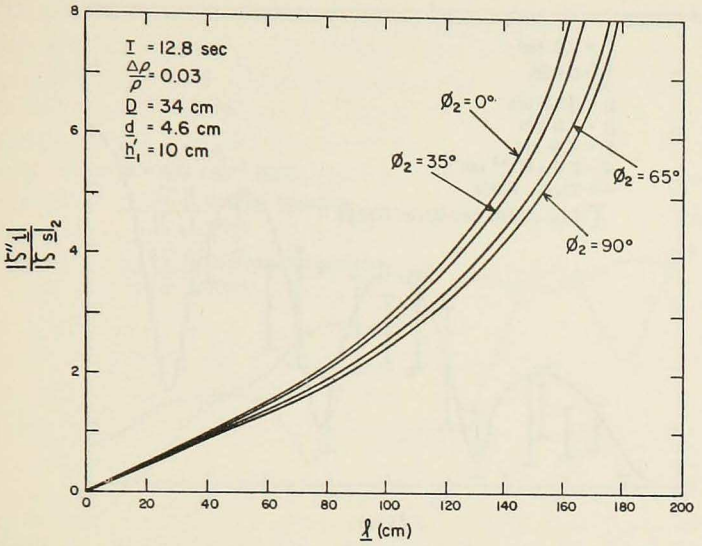

Figure 8. Ratio of internal-wave to surface-wave amplitudes of Case I for different φ_2 angles.

(25) and by the experimental points for the first case, where the interface is below the shelf depth. Ratios are absolute maximum values when the shelf width is equal to an odd number of 1/4 surface wavelengths—the resonance condition for the surface wave over the shelf area. In Fig. 6, the value of 1/4 surface wavelength is 215 cm, and the first ratio maximum is thus not reached with the available experimental shelf width; but in Fig. 7, the value is 81 cm and a maximum was found experimentally. In both figures, good agreement of the experimental values with the theoretical curves is found for the smaller amplitude ratios, *i.e.*, around nonresonance conditions at which the horizontal currents and the resulting turbulence and mixing at the shelf break are at a minimum. The deviations shown in Fig. 6 at the larger shelf widths are unexplained, but probably they are due to experimental error. Fig. 8 shows the theoretical effect of the angle φ_2—the angle made by the offshore surface-wave front with the shelf break—on the amplitude ratio for parameters similar to those in Fig. 6. The angle has little effect on the form of the curve, but it changes the position of the resonant shelf width by a factor of $\cos \varphi_1^{-1}$, which represents the increase in the x component of the surface wavelength over the shelf; for Fig. 8 it will have a value of 1.0 to 1.075 as φ_1 and φ_2 go from 0° to 19.5° and from 0° to 90°, respectively.

For the first and second parts of Case II, the interface is shallower than the shelf depth; thus there are two measurable internal-wave amplitudes: a coastal wave and an offshore progressive wave. The first part, shown in Figs. 9 and 10, has a small frictional effect ($\mu = 2.6 \times 10^{-3}$ cm^{-1}); for comparison, in Fig. 11 a second part is shown with a bigger frictional effect ($\mu = 6.0 \times 10^{-3}$

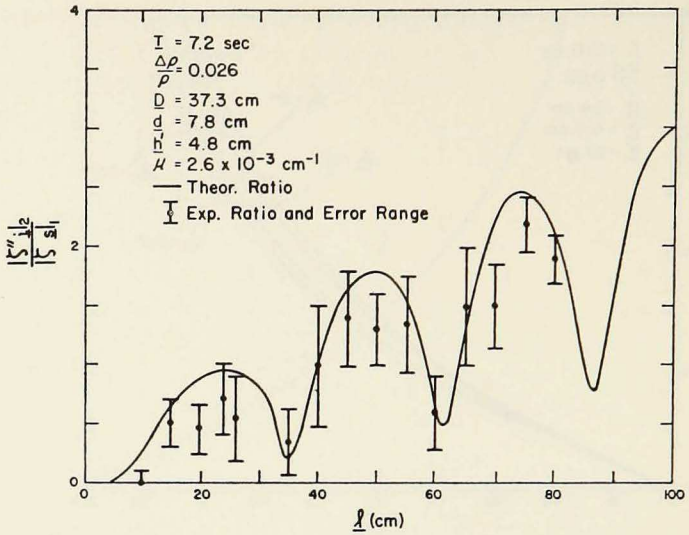

Figure 9. Theoretical and experimental ratio of offshore internal-wave to surface-wave amplitudes of Case II for small frictional effect.

cm^{-1}). Fig. 9 represents the theoretical curve and experimental data for the offshore progressive wave, which is a summation of two progressive waves traveling seaward from the shelf break. Both waves are generated at the shelf

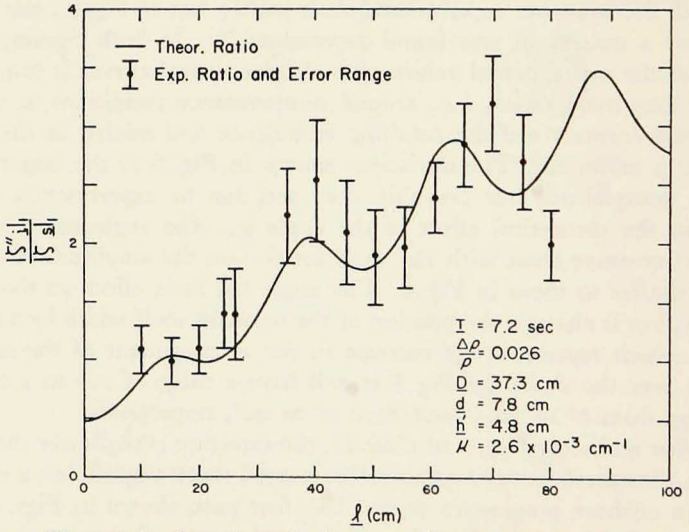

Figure 10. Theoretical and experimental ratio of coastal internal-wave to surface-wave amplitudes of Case II for small frictional effect.

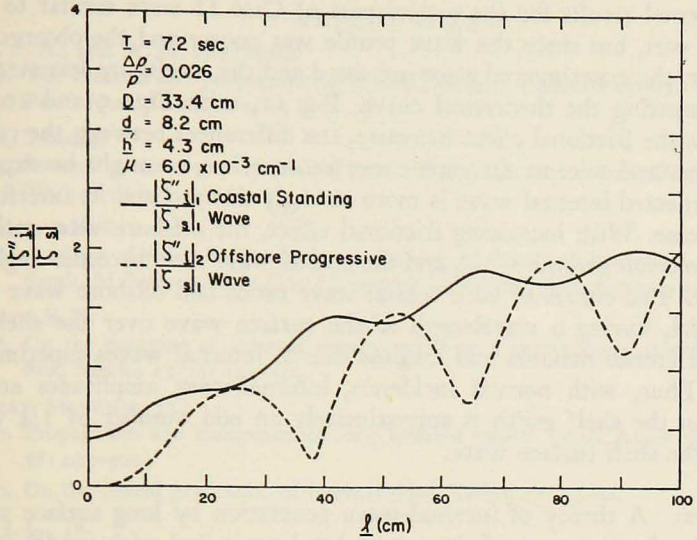

Figure 11. Ratio of internal-wave to surface-wave amplitudes of Case II for large frictional effect.

break, one traveling seaward after being reflected from the coastline. The phase relationship between the two waves is determined by the phase velocity and the shelf width while the damping of the internal wave's amplitude, as it travels over the shelf area, has an obvious importance not only to the internal wave over the shelf but also to the composite internal wave traveling seaward from the shelf. When, for normal incidence, the shelf width is an even number of 1/4 internal wavelength, the two seaward-traveling waves will be in phase; thus maximum ratio values will be found.

On the other hand, with normal incidence, resonance conditions for the coastal internal wave occur when the shelf width is an odd number of 1/4 internal wavelength, as shown in Fig. 10. The agreement of the experimental values with the theoretical curve is not so good as in Case I (Figs. 6 and 7), mainly because of the increase in mixing and because the time interval for stationary-wave conditions is shorter. Since the offshore progressive wave re-enters the observational area after being reflected from the plunger end of the wave channel, observation is limited to the time between that time when the internal-wave amplitudes first reach steady state and when the offshore wave re-enters the observation area. The observation time was about one-half that of Case I, or about 10 surface-wave periods for the first part of Case II; it was even shorter for the second part of Case II. This shorter observation time plus the poorer wave profile increased the observational error in the data. Using (49), an observational error range for each data point was calculated; this represented the greatest possible error in a data point caused by the observational uncertainties in wave amplitudes and phase angle.

Experimental results for the second part of Case II were similar to those of the first part, but since the wave profile was poorer and the observational time shorter, the experimental error increased and the results are less meaningful. By comparing the theoretical curve, Fig. 11, with Figs. 9 and 10, it is seen that, as the frictional effect increases, the differences between the consecutive maxima and minima for each curve become less, as might be expected, since the reflected internal wave is more strongly damped and its interference effects decrease. With increasing frictional effect, the offshore wave ratio approaches the result given by (24), and the coastal wave ratio becomes negligible at the coast. The curves of both coastal wave ratios and offshore wave ratios are sinusoidal, having a wavelength of the surface wave over the shelf and having interference maxima and minima due to internal waves superimposed on them. Thus, with normal incidence, internal-wave amplitudes are the largest when the shelf width is approximately an odd number of 1/4 wavelength for the shelf surface wave.

Conclusions. A theory of internal-wave generation by long surface waves, as derived in the first part of the paper, has been tested with model experiments. The results support the theory. Both theoretical and experimental results show that the effect of friction is important. The principal effect of friction is to decrease the amplitude of the internal waves traveling over the shelf. The decrease in amplitude speeds up the change from the standing-wave profile along the coast to a more progressive-wave profile traveling coastward near the shelf break; this decrease in amplitude also causes a decrease in the constructive or destructive interference of the coastal-reflected internal wave on the offshore progressive wave. With the interface either above or below the continental shelf, the offshore internal waves can be small or large, depending upon whether the shelf width approximates an even or odd multiple, respectively, of 1/4 surface wavelength.

When the interface is above the shelf, the offshore internal waves show maxima in the amplitudinal ratios when the shelf width is an even or odd multiple, respectively, of 1/4 internal coastal wavelength; but the coastal internal wave has the inverse relationship. All results were tested in the experiments, but, as the frictional effect increased, the finer features of the theoretical curves could not be verified because of an increase in the observational error. The results have shown, however, that physical models offer a practical means of studying internal waves and that it is possible to test simple fundamental theories of internal-wave generation.

REFERENCES

Davis, P. A., and A. M. Patterson

1956. The creation and propagation of internal waves, a literature survey. Tech. Memo. Pacif. Naval Lab., 56–2; 24 pp.

Ichiye, Takashi

1963. Internal waves over a continental shelf. Tech. Rep., Ocean. Inst., Florida St. Univ., No. 3; 23 pp.

Lambright, H. R.

1964. Analysis of the influence of internal waves of tidal period upon the mixed-layer depth. M.S. thesis, U.S. Naval Postgraduate School, Monterey; 23 pp.

LeBlond, P. H.

1966. On the damping of internal gravity waves in a continuously stratified ocean. J. fluid Mech., *25* (1): 121–142.

Rattray, Maurice, Jr.

1957. Propagation and dissipation of long internal waves. Trans. Amer. geophys. Un., *38*: 495–500.

1960. On the coastal generation of internal tides. Tellus, *12*: 54–62.

Reid, J. L., Jr.

1956. Observations of internal tides in October 1950. Trans. Amer. geophys. Un., *37*: 278–286.

Weigand, J. G.

1962. A model study of internal waves. M.S. thesis, Univ. of Wash., Seattle; 52 pp.

Zeilon, Nils

1913. On the seiches of Gullmar Fjord. Svensk. Hydr. Biol. Komm. Skr., *5*: 1–22.

1934. Experiments on boundary tides. Göteborgs Vetensk. Samh. Handl., Folj 5, Ser. B., *3* (10): 1–8.